Supplemental Appendix

Methods

Cloning and characterization of LA25

Human LDL was freshly isolated from plasma of healthy donors after an overnight fast by sequential ultra-centrifugation. LDL (or bovine serum albumin (BSA)) was modified with MDA plus acetaldehyde (AA) to generate MAA, or MDA alone or $CuSO_4$ to generate MAA-LDL, MAA-BSA, MDA-LDL or copper-oxidized LDL (Cu-OxLDL) respectively, as previously described in detail (1). In MAA and MDA preparations, >90% of the lysines were modified as judged using the trinitrobenzenesulfonic acid assay. While MAA-LDL preparations may contain small numbers of MDA adducts, MDA-LDL preparations usually contain few if any MAA adducts, though these may also occur in small numbers as acetaldehyde may decompose from MDA[1].

We constructed a new library (κ/λ) from lymphocytes from umbilical cord blood of 7 newborn babies and used these in the first round of screening in a method analogous to one previously described (2). The selecting epitope was MAA-BSA. MAA is a specific advanced MDA-type adduct that we and others have shown is an immunodominant MDA type epitope (3,4). After 4 rounds of panning with each library as previously described (2), we identified an enrichment in the newborn library of fully or very near germline sequences, consistent with minimal non-templated insertions in the CDR3 region. The resultant Fabs were cloned into the phagemid pComb3X as described by Barbas et al (5). LA25 was identified as a leading candidate due to its specificity for MAA epitopes and optimal expression characteristics. LA24 was identified from the same library, but did not bind any relevant oxidation-specific epitopes present in vivo. Specificity of individual phage Fab and soluble Fab were assessed by ELISA, as previously described (1,2). The specificity of Fab binding was further determined by competition chemiluminescent ELISA as described previously (2), and data expressed as B/B_o, where B represents binding in the presence and B_o in the absence of competitor. High-titer clone LA25 and control LA24 were selected and converted to the plasmid producing soluble Fab. Nucleotide and amino acid sequences of Fab clones were compared to those contained in public databases by using Ig-BLAST and IMGT/VQUEST. LA25 and LA24 plasmids from selected Fab phage clones were codon optimized and transformed into *E. coli* C41 (DE3) (Lucigen) for production of soluble Fab.

Macrophage binding experiments were performed to assess the in vivo specificity and relevance of LA25, as previously described, except that MAA-LDL was used as the antigen (6,7). Briefly, competition assays for the inhibition of biotinylated-MAA-LDL binding to macrophages by LA25 or LA24 were carried out by adding a fixed and limiting amount of biotin-MAA-LDL (5 μg/ml) to J774 macrophages in the absence or presence of increasing concentrations of LA24/LA25.

Mouse and rabbit atherosclerosis models

Female *Apoe*$^{-/-}$ mice (B6.129P2-*Apoe*^{tm1Unc}/J, 8-10 weeks old) were purchased from the Jackson Laboratory (Bar Harbor, ME) and fed a Western diet (Harlan Teklad TD.88137, 42 % calories from fat) for 22 weeks. Male New Zealand White rabbits (2.5-3.0 months old) were

purchased from Charles River Laboratories (Wilmington, MA). To promote the formation of atherosclerotic plaques, endothelial denudation of the aorta was performed after intramuscular (i.m.) administration of ketamine (20 mg/kg) (Fort Dodge Animal Health, Overland Park, Kansas, USA) and Xylazine (5 mg/kg) (Bayer AG, Leverkusen, Germany). A 4F-Fogarty embolectomy catheter (Edwards Lifesciences, Irvine, CA) was inflated at the level of the left subclavian artery and slowly deflated while retracting until the iliac bifurcation, under X-ray guidance (Philips Allura Xper FD20/10, Philips Healthcare, Best, The Netherlands), described in more detail by Lobatto et al. (8) The procedure was repeated using the contralateral femoral artery as point of entry 4 weeks after the first procedure, i.e. 6 weeks after the initiation of a high cholesterol diet (regular chow diet enriched with 0.3% cholesterol, 4.7% coconut oil, Research diets, Inc., Brunswick, NJ). After 8 weeks, diet was changed to a 0.15% enriched cholesterol diet and continued for the remaining 2.5 months before the experiments were performed. This model recapitulates some of the features of the human disease, such as raised lesions or macrophage infiltration (**Supplemental Figure 1**). Untreated healthy rabbits were fed a regular chow diet and age-matched to serve as controls. In addition, lever staining was performed on age-matched rabbits.

All animal experiments were performed in accordance with protocols approved by the Institutional Animal Care and Use Committees of the University of California, San Diego (UCSD) and the Icahn School of Medicine at Mount Sinai, and followed National Institutes of Health guidelines for animal welfare.

Immunostaining of human specimens

Human specimens from coronary atherosclerotic lesions, taken from sudden cardiac death victims, and from distal protection device debris in patients undergoing percutaneous coronary intervention, were generously provided by Dr. Virmani at the CVPath Institute and immunostained at UCSD. Hearts of patients who had died suddenly with coronary artery disease were obtained as previously described (9,10). Cases were identified retrospectively by the presence of early and late fibroatheroma, thin cap fibroatheroma and plaque rupture. Formalin-fixed, paraffin embedded coronary segments were cut at 5-µm thick sections, mounted on charged slides, and stained with hematoxylin and eosin (H&E) or the modified Movat pentachrome method as previously described (11).

Paraffin embedded tissue sections were deparaffinized with Histoclear®, rehydrated through graded ethanol, and blocked with 5% normal goat serum/1%BSA/TBS for 30 minutes. Tissues were incubated overnight at 4 ˚C with the human monoclonal antibody Fab LA25 or LA24 diluted with blocking buffer. Using the avidin–biotin–alkaline phosphatase method, tissues were incubated for 30 minutes with biotinylated monoclonal anti-HA antibody diluted with blocking buffer in a ratio of 1:1000(Sigma B9183). Tissues were then incubated with ABC Alkaline phosphatase reagent (Vector AK-5000) for 30 minutes and visualized with Vector Red substrate (Vector SK-5100). Finally, slides were then counterstained with hematoxylin for 30 seconds, dehydrated through graded ethanol, cleared with Histoclear and a coverslip was adhered using histomount. Immunostaining of adjacent sections in the absence of primary Fab were used as negative controls.

Distal protection devices were obtained from 24 patients undergoing clinically indicated coronary and peripheral procedures as previously described (12). At the end of the procedure,

the recovered filters from the distal protection devices were placed in ice-cold phosphate buffered solution containing EDTA/BHT (4μM/20μM). The filter bottom was cut off, the filter inverted and the material was paraffin embedded en bloc. Filters were chosen that had visible (yellow/white) material at bottom of filter. Seven μm serial sections were prepared, rehydrated, and immunostained with antibodies LA25 and LA24. The collection of materials was approved by the UCSD Human Research Subjects Protection Program.

Radiolabeling of Fab LA25 and non-specific isotype control Fab LA24

Modification of LA24 and LA25 for labeling with ^{89}Zr was carried out as previously reported (13). Briefly, to a solution of LA24 or LA25 Fab (1-2 mg/ml) in 0.1 M carbonate buffer, pH 8.7-8.9, was added *p*-isothiocyanatobenzyl-desferrioxamine (Macrocyclics, Plano, TX; 5 mg/ml in DMSO) until a 2:1 mol ratio was achieved. The mixture was reacted at 37° C for 2 h, then allowed to cool down to room temperature. The DFO-modified Fab was purified by centrifugal filtration using 10 kDa molecular weight cut-off (MWCO) filter tubes and washing twice with ample fresh PBS to prevent excessive concentration. For radiolabeling, the DFO-bearing Fabs were reacted with [^{89}Zr] Zirconium (IV) oxalate in PBS pH 7.1-7.4 for 2 h. After cooling down, the radiolabeled Fabs were purified by gel filtration using PD-10 columns and PBS as eluent. The radiochemical yield was 86 ± 9 % (n = 6), and the radiochemical purity 96 ± 8 % (n = 6), as assessed by size exclusion chromatography (**Supplemental Figure 2A**). The specific activities were 2.7 ± 0.1 mCi/mg (n = 2) and 3.8 ± 0.4 mCi/mg (n = 3) for ^{89}Zr-LA24 or ^{89}Zr-LA25, respectively.

Pharmacokinetics and biodistribution of ^{89}Zr-LA24 and ^{89}Zr-LA25 in mice

Pharmacokinetic profile and biodistribution evaluation of the PET tracer ^{89}Zr-LA25 was carried out in *Apoe*$^{-/-}$ mice (n=13, mean weight 30.8 ± 6.8 g), using ^{89}Zr-LA24 as chemical control. Radioactivity half-life was determined in blood after lateral tail-vein injection. Animals were injected with ^{89}Zr-LA25 or ^{89}Zr-LA24 (23 ± 1 μCi, 6-8 μg). Blood was drawn from the tail vein at 1, 30, 60, 120, 180, and 240 minutes after injection. Blood was weighted and counted using a Wizard^2 2480 automatic gamma counter (Perkin Elmer, Waltham, MA). At 4 hours after injection, all mice were sacrificed using an overdose of isoflurane (Baxter, Deerfield, IL) and perfused through the heart with 20 ml saline. The following organs were harvested: brain, heart, lung, spleen, liver, kidneys, skeletal muscle and bone were harvested and weighted before counting using a Wizard^2 2480 automatic gamma counter. Radioactivity concentration in tissues was calculated as percentage of injected dose per gram (%ID/g).

Immunofluorescence of mouse aortic roots

Aortic mouse roots were harvested 4 hours after injection, put in optimal cutting temperature (OCT) and cut in 7 μm thick sections. The first slide was subjected to autoradiography, while adjacent sections were stained for macrophages (CD68, red) and endothelial cells (CD31, green). Additional nuclear staining was performed using 4',6-Diamidino-2-phenylindole dihydrochloride (DAPI, Sigma Aldrich, St. Louis, MO). All images were obtained using an EVOS FL Auto digital inverted fluorescence microscope (Life Technologies, Norwalk, CT). Fluorescent images were obtained at 4× magnification, while brightfield images were obtained at both the 4× and 20× magnification. On stained sections, CD68 fluorescence was

observed using a Texas Red light cube (Ex 585/29, Em 624/40, EVOS LED Light cube), while CD31 fluorescence was observed using a GFP light cube (Ex 470/22, Em 510/42, EVOS LED Light cube).

Immunostaining of mouse and rabbit livers

Rabbit and mouse livers were harvested and put in formalin before re-embedding in paraffin < 72 hours after harvest. The liver specimens were subsequently stained according to the same protocol as described for human specimens.

PET/MR imaging

Rabbits (n=12, mean weights: 3.4 ± 0.9 kg for rabbits with atherosclerosis, and 3.2 ± 0.1 kg for healthy control rabbits). A 24G-catheter was introduced in the marginal ear vein for injection with either ^{89}Zr-LA25 or ^{89}Zr-LA24 (0.94 ± 0.22 mCi, 0.3-0.4 mg). In the contralateral ear, a 22G-catheter was used for the administration of the gadolinium based contrast agent; gadopentetate dimeglumine (Magnevist, Bayer Healthcare). Anesthesia was induced by intramuscular injection of Ketamine (20 mg/kg) (Fort Dodge Animal Health, Overland Park, Kansas, USA), together with Xylazine (0.5 mg/kg) (Bayer, Shawnee Mission, Kansas, USA). Prior to ^{18}F-FDG injections rabbits were fasted for at least 4 hours. All rabbits received a urine catheter to prevent any disruptions from signal in the bladder.
Rabbits were placed in a body matrix coil and received isoflurane anesthesia at 1.5% by inhalation and were oxygenated for the remaining of the PET/MR imaging experiment, while vital parameters were monitored. Shortly after injection, images were acquired in a dynamic fashion for the duration of 1 hour using a clinical 3 Tesla PET/MRI Biograph mMR (Siemens, Munchen, Germany). After scout scans, the PET scan was initiated and co-acquired with a radial VIBE MR sequence with the following imaging parameters: TR, 20 ms; TE, 1.89 ms; flip angle, 10 degrees; slice thickness, 1.1 mm^3. Attenuation correction of PET images was done using the built-in MR-based attenuation correction (MR-AC) map and images reconstructed using the OP-OSEM algorithm. In addition, a time-of-flight (TOF) non-contrast enhanced angiography was performed for localization of arterial anatomical landmarks (renal arteries and iliac bifurcation). Imaging parameters were: TR, 1600 ms; TE, 118 ms; flip angle, 140 degrees; ETL, 83; slice thickness, 0.6 mm.

A dynamic contrast-enhanced MRI (DCE-MRI) scan was performed. Black blood was obtained using a double inversion recovery (DIR) technique. A 3D turbo field echo (TFE) sequence with motion sensitized driven equilibrium (MSDE) preparation for black blood imaging was used to quantify the uptake of a FDA approved gadolinium based CA; gadopentetate dimeglumine (Magnevist, Bayer Healthcare) from the right renal artery to the iliac bifurcation. This protocol of black blood DCE-MRI is explained in more detail by Calcagno et al. (14) Imaging parameters were: TR, 6.2 ms; TE, 2.8 ms; flip angle, 20 degrees; ETL, 80; spatial resolution, 0.6 mm3; FOV, 160 mm2; 20 slices; orientation, sagittal. This sequence was used before and 10 minutes after CA injection to quantify the CA accumulation in the vessel wall and thus to measure the permeability of the vessel wall. Before and during CA injection, the same sequence was used with 3 signal averages (time resolution 32s) to perform 3D DCE-MRI, and quantify the rate of uptake of CA in the vessel wall. The next day, 24 ± 1.5 hours after injection, all rabbits received a 20 minutes static PET-scan, again using a TOF and MR-AC.

Pharmacokinetics and biodistribution ^{89}Zr-LA25 or ^{89}Zr-LA24 in rabbits

Radioactivity half-lives were determined by drawing blood from the ear arteries at 1 and 30 minutes, and at 1, 2, 4, 20, 24 and at sacrifice after 28 hours. All rabbits were sacrificed by an i.v. injected overdose of 100 mg/kg sodium pentobarbital and subsequently perfused with 500ml saline. After sacrifice, all animals were perfused to make sure no blood or blood clots remained in the aorta and other organs before excision. Aortas were excised and divided in thoracic, form the aortic root until the diaphragm and the abdominal aorta, infra-diaphragmatic until iliac bifurcation, the latter with celiac trunk and renal arteries attached, serving as landmarks. The following organs were harvested: heart, lungs, liver, spleen, kidneys, one adrenal gland, muscle and bone-marrow and were weighted. All tissues were weighted before counting with a Wizard2 2480 automatic gamma counter. Radioactivity concentration in tissues was calculated as percentage of injected dose per gram (%ID/g).

Near-infrared fluorescence imaging

Twenty-four hours before sacrifice, all rabbits received fluorescently labeled high-density lipoprotein (DiD-HDL, ~1 mg dye per rabbit) in 5 ml PBS solution via the marginal ear vein. After sacrifice all aortas, thoracic and abdominal, were placed on thick black paper and imaged with a Xenogen IVIS-200 optical imaging system (Perkin Elmer, Waltham, MA). Fluorescence images were acquired with excitation and emission wavelengths of 680 and 720 nm and a field of view (FOV) of 6.5 cm and 22.8 cm using different exposure times.

Autoradiography

Aortas were placed in a film cassette against a phosphorimaging plate (BASMS-2325, Fujifilm, Valhalla, NY) for 48 h (mouse aortas, rabbit organs) or 72 h (rabbit aortas) at -20 °C to determine radiotracer distribution. Luminal autoradiography was performed for 96 h, after one of the harvested aortas was cut into 20µm thick sections. Phosphorimaging plates were read at a pixel resolution of 25 µm with a Typhoon 7000IP plate reader (GE Healthcare, Pittsburgh, PA).

Image analysis

Image analysis for PET-imaging was performed after all data were processed and divided in different time frames using a custom-made program written in Matlab (Mathworks, Natick, MA). All data was subsequently processed using OsiriX Imaging Software (OsiriX Foundation, Geneva, Switzerland) by drawing regions of interest (ROIs) on the infrarenal abdominal aorta, and major organs (liver, spleen and kidneys). By averaging all acquired ROIs per organ (≥10 per organ), mean SUV_{max} values in each tissue were obtained. All images acquired with DCE-MRI were reformatted in the axial plane for tracing. The vessel wall tracing was made on the average image of the dynamic series of DCE-MRI using Osirix software (OsiriX Foundation, Geneva, Switzerland). By drawing an inner and an outer vessel wall contour and computing the difference between these two, the vessel wall area or Region of Interest (ROI) was measured. The area under the normalized signal intensity curve (IAUC) was calculated after two minutes, serving as a time point for data analysis, with a custom-made program written in Matlab (Mathworks, Natick, MA). IAUC is a measure of contrast agent extravasation and uptake in the (atherosclerotic) vessel wall. IAUC was calculated on a pixel-by-pixel basis. MR signal intensity

over time was normalized to vertebral muscle signal intensity before the injection of contrast agent. NIRF analysis was done using Living Image Software (Perkin Elmer, Waltham, MA). All thoracic and abdominal aortas were divided in 10 equal regions of interest and quantified as Total Radiant Efficiency in [p/s]/[μW/cm^2].

Histological analysis and immunostaining of rabbit aortic sections

Sections of 0.5 cm from the excised abdominal aorta were placed in optimal cutting temperature (OCT) compound and were cut into 7μm thick sections that were adjacent to the luminal autoradiography cut section. Sections were stained for hematoxylin and eosin, RAM-11 for macrophages or Oil Red O for lipids (Dako, Santa Clara, CA) according to previous used methods (15). Detailed images were made with a Nikon Eclipse E400 microscope, a Nikon DS-U1 camera box, and a Nikon DS-5 M camera while whole luminal aorta images were made using an Olympus Stereoscope MVX10.

Statistics

Statistical analysis was conducted using nonparametric Mann-Whitney tests. Spearman's r coefficients were calculated to determine the degree of correlation. Data are reported as mean ± standard deviation. *P* values of < 0.05 were considered statistically significant. Prism software (version 6.0, GraphPad Software Inc., La Jolla, CA) was used to calculate the different statistical parameters.

Supplemental Figure 1. Histological staining of healthy (top) and atherosclerotic (bottom) rabbit aorta sections. Left panels show conventional hematoxylin and eosin (H&E) staining, middle shows CD31 immunostaining for endothelial cells (indicative of neovessels in the adventitia in the atherosclerotic aorta) and the right panel shows RAM-11 immunostaining for macrophages, indicating more macrophages in the atherosclerotic sections. * Indicates lumen of the vessel.

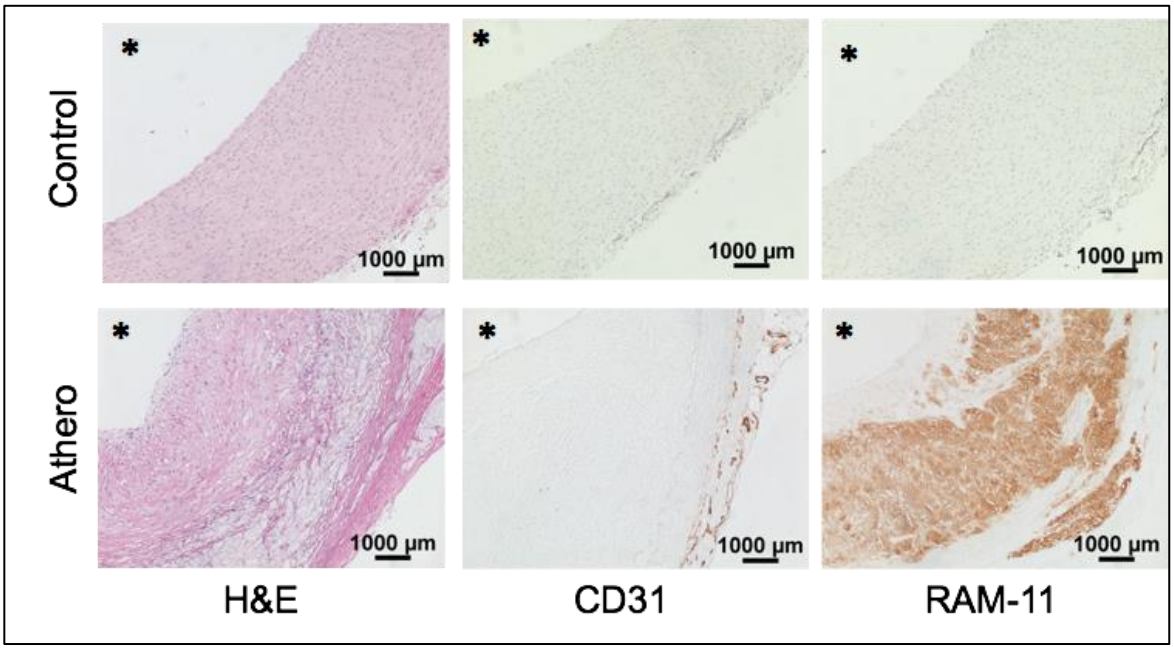

Supplemental Figure 2. Size exclusion chromatograms of ^{89}Zr-LA25 and ^{89}Zr-LA24, showing co-elution of unlabeled (black, UV trace) and radiolabeled Fab (dark grey, radioactive trace). The radioactive trace of free, uncomplexed ^{89}Zr is also shown for reference (light grey). (**A**). Biodistribution in *Apoe*$^{-/-}$ mice as measured by *ex vivo* gamma counting 4 h after injection with either ^{89}Zr-LA24 (grey) or ^{89}Zr-LA25 (black). Ki=kidney; Li=liver; Sp=spleen; Bl=blood; Lu=lungs; Bo=bone; He=heart; Mu=muscle; Br=brain. Radioactivity concentration in tissues was calculated as percentage of injected dose per gram of tissue (%ID/g), * P<0.05 (**B**).

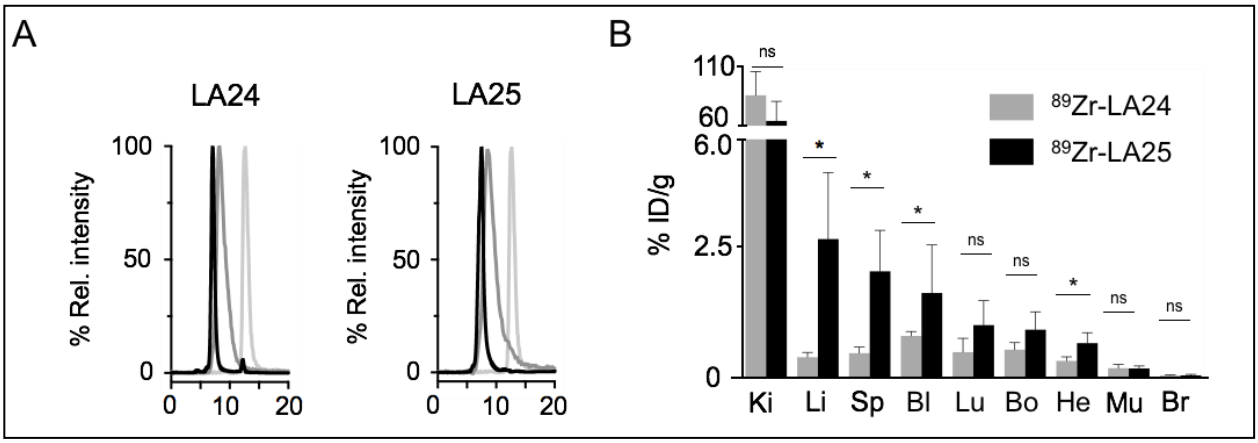

Supplemental Figure 3. Representative coronal PET images of rabbits at 20, 40 and 60 minutes and at 24 hours post injection of ^{89}Zr-LA25 and ^{89}Zr-LA24. Fused PET/MR images are shown on the right of each row. The top row shows ^{89}Zr-LA25 in healthy control rabbits, middle row ^{89}Zr-LA25 in atherosclerotic rabbits and bottom row ^{89}Zr-LA24 in atherosclerotic rabbits.

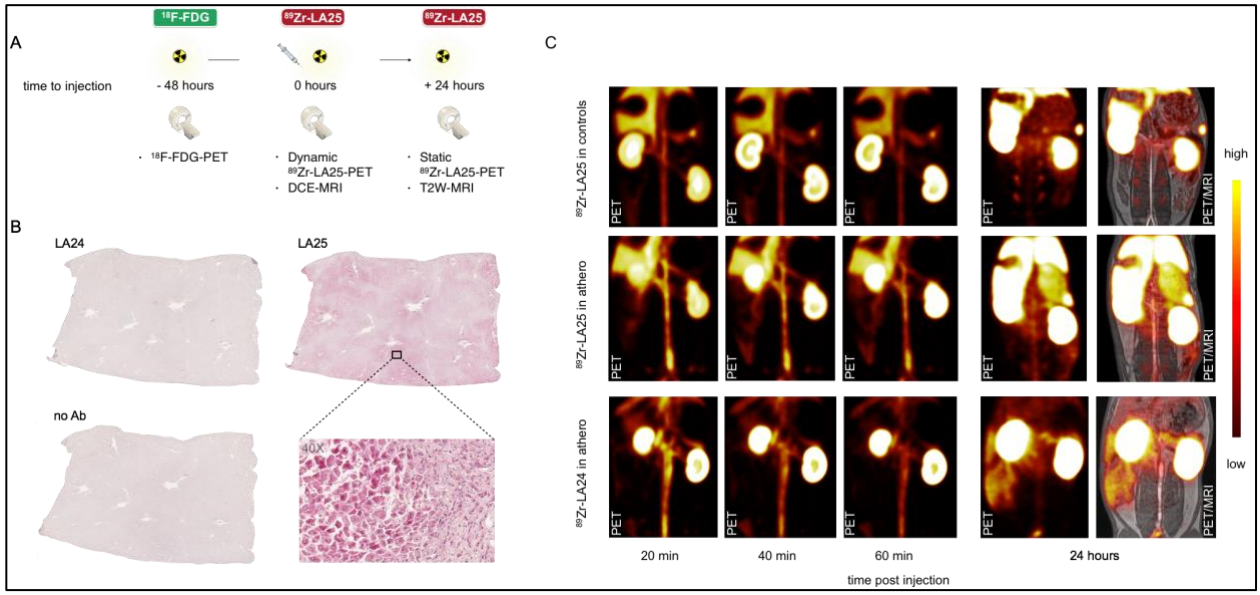

Supplemental Figure 4. Biodistribution in atherosclerotic rabbits as measured by *ex vivo* gamma counting 28 h after injection with either ^{89}Zr-LA24 (grey) or ^{89}Zr-LA25 (black) (**A**). Blood time-activity curve for ^{89}Zr-LA25 in healthy controls and atherosclerotic rabbits, with half-lives of 1.3 and 2.2 h, respectively (**B**). Correlation between target-to-blood ratio (TBR) values of aortas as determined by PET (as ratio to withdrawn blood at time of scanning, 24 hour post injection) and gamma counting for both ^{89}Zr-LA25 and ^{89}Zr-LA24 injected rabbits (P<0.0001) (**C**). Ki=kidney; Sp=spleen; BM=bone marrow; Ad=adrenal glands; Li=liver; Ao=aorta; Lu=lungs; He=heart; Bl=blood; Mu=muscle. Radioactivity concentration in tissues was calculated as percentage of injected dose per gram (%ID/g), * P<0.05.

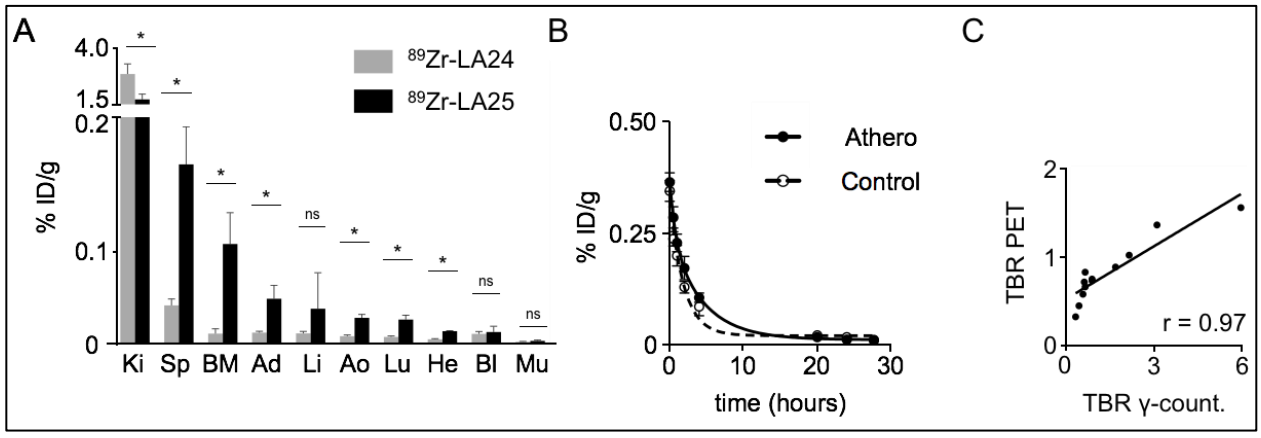

Supplemental Figure 5. Representative aortas of atherosclerotic rabbits injected with ^{89}Zr-LA25, showing autoradiography (left) and near infrared fluorescence (NIRF) imaging after DiD-rHDL injection in the same rabbit (right), revealing a similar distribution pattern (**A**). A significant positive correlation between ^{89}Zr-LA25 radioactivity, measured by gamma counting, and fluorescent rHDL NIRF intensity in aortas, defined as total radiant efficiency, was found (r=0.83, *P*=0.02). This was repeated for rabbits injected with ^{89}Zr-LA24 (**B**).

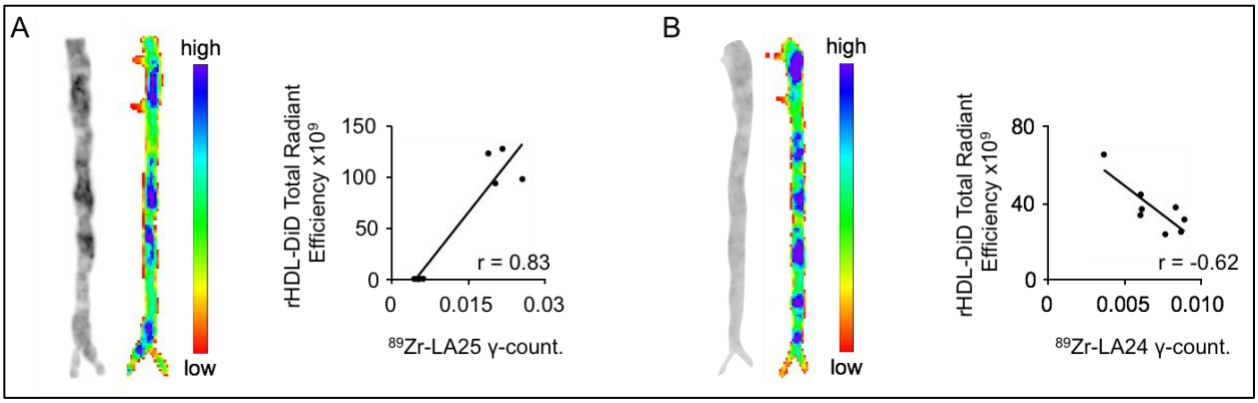

Supplemental Figure 6. Correlations between PET-measured ^{18}F-FDG uptake and rHDL NIRF intensity in rabbit aortas (r=0.67, *P*<0.0001) (**A**), and between *ex vivo* quantified ^{89}Zr-LA25 uptake and (i) PET-derived ^{18}F-FDG uptake (r=0.79, *P*=0.03) (**B**), (ii) plaque area as determined by T2-weighted MRI (r=0.83, *P*=0.02*)* (**C**), and (iii) permeability as determined by DCE-MRI (r=0.57, *P*=0.15*)* (**D**). SUV: standardized uptake value. IAUC: area under the normalized signal intensity curve.

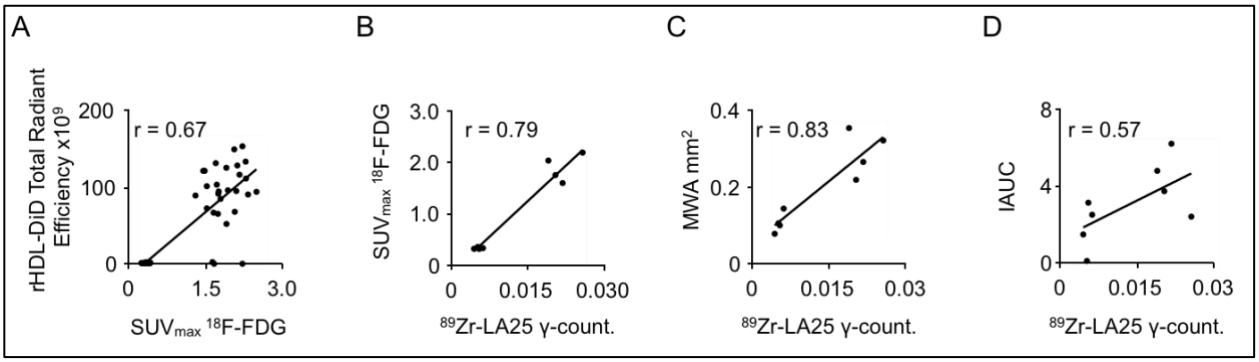

Supplemental Figure 7. Cardiac PET/MR images in rabbits with atherosclerosis after ^{18}F-FDG (*top*) or ^{89}Zr-LA25 (*bottom*) injection (A), and associated aorta-to-heart ratios (B).

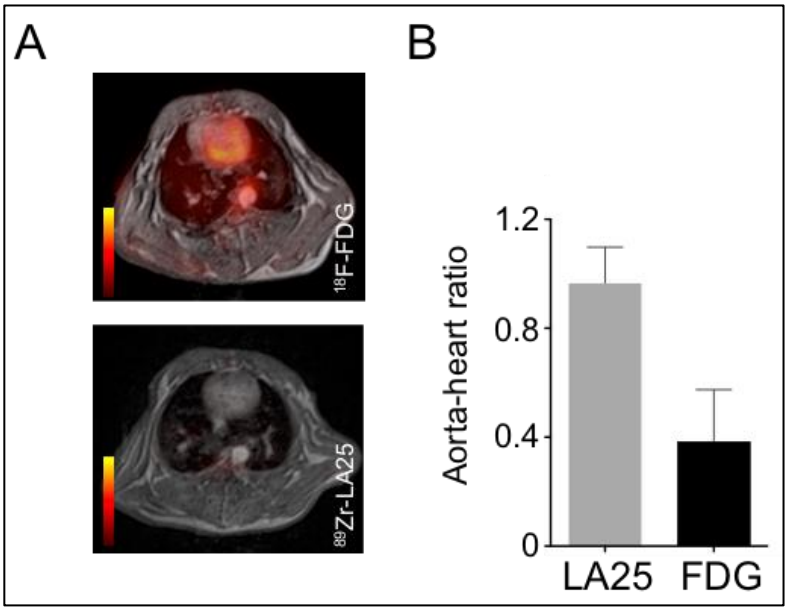

References

1. Gonen A, Hansen LF, Turner WW, Montano EN, Que X, Rafia A, Chou MY, Wiesner P, Tsiantoulas D, Corr M, VanNieuwenhze MS, Tsimikas S, Binder CJ, Witztum JL and Hartvigsen K. Atheroprotective immunization with malondialdehyde-modified LDL is hapten specific and dependent on advanced MDA adducts: implications for development of an atheroprotective vaccine. J Lipid Res 2014;55:2137-55.
2. Shaw PX, Horkko S, Tsimikas S, Chang MK, Palinski W, Silverman GJ, Chen PP and Witztum JL. Human-derived anti-oxidized LDL autoantibody blocks uptake of oxidized LDL by macrophages and localizes to atherosclerotic lesions in vivo. Arterioscler Thromb Vasc Biol 2001;21:1333-9.
3. Weismann D, Hartvigsen K, Lauer N, Bennett KL, Scholl HP, Charbel Issa P, Cano M, Brandstatter H, Tsimikas S, Skerka C, Superti-Furga G, Handa JT, Zipfel PF, Witztum JL and Binder CJ. Complement factor H binds malondialdehyde epitopes and protects from oxidative stress. Nature 2011;478:76-81.
4. Niemela O, Parkkila S, Yla-Herttuala S, Halsted C, Witztum JL, Lanca A and Israel Y. Covalent protein adducts in the liver as a result of ethanol metabolism and lipid peroxidation. *Lab Invest*. 1994;70:537-46.
5. Barbas CF, III and Lerner RA. Combinatorial immunoglobulin libraries on the surface of phage (phabs): Rapid selection of antigen-specific fates. Methods 1991;2:119-124.
6. Tsimikas S, Miyanohara A, Hartvigsen K et al. Human oxidation-specific antibodies reduce foam cell formation and atherosclerosis progression. J Am Coll Cardiol 2011;58:1715-27.
7. Montano EN, Boullier A, Almazan F, Binder CJ, Witztum JL, Hartvigsen K. Development and application of a nonradioactive binding assay of oxidized low-density lipoprotein to macrophage scavenger receptors. J Lipid Res 2013;54:3206-14.
8. Lobatto ME, Calcagno C, Metselaar JM, Storm G, Stroes ES, Fayad ZA, Mulder WJM. Imaging the efficacy of anti-inflammatory liposomes in a rabbit model of atherosclerosis by non-invasive imaging. Methods Enzymol 2012;508:211-28.
9. Kramer MC, Rittersma SZ, de Winter RJ, Ladich ER, Fowler DR, Liang YH, Kutys R, Carter-Monroe N, Kolodgie FD, van der Wal AC and Virmani R. Relationship of thrombus healing to underlying plaque morphology in sudden coronary death. J Am Coll Cardiol 2010;55:122-132.
10. van Dijk RA, Kolodgie F, Ravandi A, Leibundgut G, Hu PP, Prasad A, Mahmud E, Dennis E, Curtiss LK, Witztum JL, Wasserman BA, Otsuka F, Virmani R and Tsimikas S. Differential expression of oxidation-specific epitopes and apolipoprotein(a) in progressing and ruptured human coronary and carotid atherosclerotic lesions. J Lipid Res 2012;53:2773-90.
11. Farb A, Weber DK, Kolodgie FD, Burke AP and Virmani R. Morphological Predictors of Restenosis After Coronary Stenting in Humans. Circulation 2002;105:2974-2980.
12. Ravandi A, Leibundgut G, Hung MY, Patel M, Hutchins PM, Murphy RC, Prasad A, Mahmud E, Miller YI, Dennis EA, Witztum JL and Tsimikas S. Release and capture of bioactive oxidized phospholipids and oxidized cholesteryl esters during percutaneous coronary and peripheral arterial interventions in humans. J Am Coll Cardiol 2014;63:1961-71.
13. Vosjan MJ, Perk LR, Visser GW, Budde M, Jurek P, Kiefer GE and van Dongen GA. Conjugation and radiolabeling of monoclonal antibodies with zirconium-89 for PET imaging

using the bifunctional chelate p-isothiocyanatobenzyl-desferrioxamine. Nat Protoc 2010;5:739-43.
14. Calcagno C, Lobatto ME, Dyvorne H et al. Three-dimensional dynamic contrast-enhanced MRI for the accurate, extensive quantification of microvascular permeability in atherosclerotic plaques. NMR Biomed 2015;28:1304-14.
15. Zhang Z, Machac J, Helft G, Worthley SG, Tang C, Zaman AG, Rodriguez OJ, Buchsbaum MS, Fuster V, Badimon JJ. Non-invasive imaging of atherosclerotic plaque macrophage in a rabbit model with F-18 FDG PET: a histopathological correlation. BMC Nucl Med 2006;6:3.